journal of the mechanical behavior of biomedical materials 141 (2023) 105773

Contents lists available at ScienceDirect

Journal of the Mechanical Behavior of Biomedical Materials

journal homepage: www.elsevier.com/locate/jmbbm

Boron nitride decorated poly(vinyl alcohol)/poly(acrylic acid) composite nanofibers: A promising material for biomedical applications

Deniz Doğan [a], F. Rabia Karaduman [b], Nesrin Horzum [c], Ayşegül Ülkü Metin [a,*]

[a] Department of Chemistry, Faculty of Science and Arts, Kırıkkale University, Yahşihan, 71450, Kırıkkale, Turkey
[b] Graduate School of Natural and Applied Sciences, İzmir Katip Çelebi University, İzmir, 35620, Turkey
[c] Department of Engineering Sciences, Izmir Katip Çelebi University, Izmir, Turkey

ARTICLE INFO

Keywords:
Electrospun fiber
Boron nitride
Mechanical
Thermal and biological properties

ABSTRACT

In this study, polyvinyl alcohol (PVA) and polyacrylic acid (PAA) nanofibers loaded with boron nitride nanoparticles (mBN) were fabricated by using electrospinning and crosslinked by heat treatment. The physical, chemical, and mechanical properties, hydrophilic behavior, and degradability of composite nanofibers were evaluated. The mechanical properties such as elastic modulus, elongation percentage at the break, and mechanical strength of PVA/PAA nanofibers improved with mBN loading. The thermal conductivity of composite nanofibers reached 0.12 W/m·K at mBN content of 1.0 wt% due to the continuous heat conduction pathways of mBN. In the meantime, while there was no cytotoxicity recorded for both L929 and HUVEC cell lines for all composite nanofibers, the antimicrobial efficiency improved with the incorporation of mBN compared with PVA/PAA and recorded as 68.8% and 75.1% for *Escherichia coli* and *Staphylococcus aureus*, respectively. On this basis, the present work proposes a promising biomaterial for biomedical applications such as dual drug delivery, particularly including both hydrophobic and hydrophilic drugs or wound dressing.

1. Introduction

Nanotechnology-based products have become the backbone of many technological developments (Sridhar et al., 2014). Polymeric nanocomposites obtained from a combination of polymer-based nanostructures (i.e. micelles, nanoparticles, nanofibers, nanobubbles, dendrimers) and nanofillers (i.e. carbon nanotubes, graphite, boron nitride) used to support the polymer and provide better properties are preferred for various applications (Gonzalez-Ortiz et al., 2020; Xiong et al., 2021; Yadav et al., 2018). Among them, nanofibers are widely preferred to be used in many biomedical and industrial fields, such as wound healing (J. J. Wang et al., 2018), tissue regeneration scaffolds (Sridhar et al., 2014) biosensors (Al-Dhahebi et al., 2020), air and water filtration (Sundaran et al., 2019), fuel cell membranes, photovoltaic semiconductor electrodes, catalysts, and piezoelectrics (Bhardwaj and Kundu, 2010; Nisbet et al., 2009; Schiffman and Schauer, 2008; Teo et al., 2011).

Electrospinning, one of the techniques used to fabricate continuous nanofibers, transforms high molar mass polymers into stable and uniform polymeric fibers with diameters ranging from nanometers to micrometers under high voltage (Chee et al., 2021; Huang et al., 2003; Li and Xia, 2004; J. Xie et al., 2021). In recent years, ultrafine nanofibers have been successfully obtained from solution or molten forms. Electrospun nanofibers at micro or nano scales exhibit exceptional properties such as high surface area to volume ratio, uniform porosity, and flexibility compared to other material forms. They can mimic the structure of the extracellular matrix, which is essential for epithelial cell growth and proliferation and accelerates the formation of new skin (Ambekar and Kandasubramanian, 2019; Arafat et al., 2021). The flexibility of the nanofiber structure allows also the healing of irregular wounds (Arafat et al., 2021; Pan et al., 2019). Biocompatible polymers such as polyvinyl alcohol (PVA), polyacrylic acid (PAA), poly (2-hydroxyethyl methacrylate) (pHEMA), and poly(*N*-isopropyl acrylamide) (PNIPAm) are frequently used in electrospinning (Chee et al., 2021; Laftah et al., 2011). To improve the properties of electrospun nanofibers, metal or ceramic nanoparticles such as graphene (Bao et al., 2010), silica (Horzum et al., 2012; Zhu et al., 2018), silver (L. Huang et al., 2022), gold (Ge et al., 2022), multi-walled carbon nanotube (Yun et al., 2011), and BN (Gu et al., 2017; Kim et al., 2018; Yin et al., 2019) have been used. The incorporation of nanoparticles into polymers leads to the emergence of functional materials used in many areas affecting electrical conductivity, reducibility, and antimicrobial and mechanical

* Corresponding author.
E-mail address: aumetin@kku.edu.tr (A.Ü. Metin).

https://doi.org/10.1016/j.jmbbm.2023.105773
Received 18 January 2023; Received in revised form 5 March 2023; Accepted 7 March 2023
Available online 8 March 2023

properties of materials (Li et al., 2018; Sun et al., 2017; C. C. Wang et al., 2017).

Hexagonal BN has become the focus of researchers in recent years with its high thermal conductivity, superior thermal stability, and excellent mechanical properties (Golberg et al., 2010; Li et al., 2018). BN nanolayers, BN nanotubes (BNNTs), and BN nanoplatelets have been used as nanofillers to improve the mechanical and thermal conductivity of various materials (Jing et al., 2017; Khan et al., 2013; Zhi et al., 2009). In addition, they are promising materials in the biomedical field due to their good biocompatibility (Merlo et al., 2018; Mukheem et al., 2019). It has been shown that biodegradable nanocomposites reinforced with BNNTs increase the scaffold's durability, while they have a non-toxicity on osteoblasts and macrophages, and supports also cell proliferation (Lahiri et al., 2010, 2011). BN nanomaterials with or without functionalization have been used as nanofiller to enhance the aforementioned properties of various polymeric films or nanofibers such as polyvinyl alcohol (Duan et al., 2013; Yin et al., 2019), cellulose (Hu et al., 2020, 2022), chitosan (W. W. Huang et al., 2022; Kaya et al., 2022), polyacrylonitrile (He et al., 2021), polyvinyl butyral (Alva et al., 2018), poly(*N*-methylpyrrole) (PNMPy) (Yegin et al., 2022), pHEMA (Doğan and Metin, 2022), poly (methyl methacrylate) (M. M. Li et al., 2022), polyvinylidene fluoride (Sekkarapatti Ramasamy et al., 2021; Zhang et al., 2018), and PVA/PAA(Kim et al., 2018).

PVA/PAA electrospun nanofibers have a well-shaped cross-linked hydrophilic structure with a high absorption capacity for water and biological fluid. Due to the strong hydrogen bonds between PVA and PAA, they can be used as wound dressings (Arafat et al., 2021; Serinçay et al., 2013; Zhan et al., 2021), adsorbents for wastewater treatment (Kim et al., 2019; Z. Z. Li et al., 2022; Park et al., 2017; J. Xie et al., 2021; Zhang et al., 2019), and solid polymer electrodes for electrochemical systems (Wu et al., 2006).

Meanwhile, the physicochemical properties of PVA/PAA nanofibers have been improved by incorporating nanofillers such as carbon nanotube, silica, or hydroxyapatite (Hejabri Kandeh et al., 2021; Kim et al., 2019; Yun et al., 2011; Zhu et al., 2018).

The applications of undoped or doped PVA/PAA nanofibers in the literature are mostly for water treatment. In this study, the structural, thermal, and mechanical properties of BN-doped nanofibers were evaluated and their potential to be used as wound dressings was investigated.

Although BN has been used in the production of PVA-based film or nanofibers, its usage as a nanofiller in PVA/PAA blend electrospun nanofiber is limited. Kim et al. fabricated the amine-functionalized BNNTs reinforced-PVA/PAA nanofibers and reported alteration of composite nanofiber's thermal conductivity (Kim et al., 2018).

Therefore, our study describes, the effect of BN on the physicochemical and biological properties of PVA/PAA nanofibers for the first time. Herein, to improve dispersibility into a matrix, hexagonal BN firstly exfoliated in an alcohol medium using simple ultrasonic treatment, then hydroxlated-BN (mBN) incorporated PVA/PAA nanofibers with different amount of loading were fabricated by electrospinning. The morphology of the composite nanofibers was analysed by microscopy techniques. Thermal and mechanical stability, thermal conductivity of composite nanofibers were described. The properties of wettability and swelling degree of nanofibers were also evaluated. Finally, the electrospun nanofibers were utilized in terms of in-vitro cytotoxicity, hemocompatibility, and antibacterial efficacy to ensure biological functionality.

2. Materials and methods

2.1. Chemicals

Polyvinyl alcohol (PVA, Mn ~30.000–70.000 g/mol, 87–90% hydrolyzed) and polyacrylic acid (PAA, Mw~450.000 g/mol) were purchased from Merck. Boron nitride (BN, 50 nm, 99.9%) was obtained from Nanotech, Turkey.

2.2. Modification of BN

BN nanoparticles were prepared using a previously reported method based on sonication-assisted exfoliation (Liu et al., 2020). Briefly, BN nanoparticles were dispersed in 40 mL of ethanol in an ultrasonic bath (600W) for 30 min and centrifuged at 5000 rpm for 5 min. Then, the supernatant was separated, washed three times with deionized water, and dried. The modified product was denoted as mBN.

2.3. Fabrication of mBN-PVA/PAA nanocomposite fibers

2.3.1. Polymer solution preparation

Aqueous PVA and PAA solutions were prepared according to a previously described method in the literature (Arik et al., 2019). Briefly, for the PVA solution, 3.50 g PVA was dissolved in 28.0 mL of deionized water with magnetically stirring for 3 h. When the PVA solution was completely dissolved, PAA solution (8 wt%, 1.30 g in 15.0 mL) was added into the PVA solution to achieve a final polymer concentration of 10 wt%.

For the preparation of mBN containing electrospun nanofibers, the mBN was added to PVA/PAA solution in different ratios (0.5, 1, 2, and 5 wt%). The polymer/mBN solution was firstly incubated in an ultrasonic bath (180 W) for 15 min, and then stirred magnetically for 2 h.

2.3.2. Preparation of electrospun nanofibers

Electrospinning device (Inovenso Basic Set-up) was used by adjusting the flow rate as 1 mL/h with the help of a microinfusion pump. A voltage of about 20 kV and a 20 cm needle-to-collector distance were provided. Each polymeric solution (PVA/PAA and mBN containing PVA/PAA polymeric solutions) was electrospun for 4 h to control the thickness of the mats (~200 μm).

The mBN-PVA/PAA composite nanofibers were denoted as mBN0.5-PVA/PAA; mBN1-PVA/PAA; mBN2-PVA/PAA; mBN5-PVA/PAA according to the ratio of mBN loading. The electrospun nanofibers samples (PVA/PAA and all mBN-PVA/PAA) were annealed at 135 °C for 80 min to obtain water-stable nanofibers.

2.4. Characterization studies

2.4.1. Microscopy analysis

The morphology of BN nanoparticles was determined using a transmission electron microscope (TEM, JEM 2100F, Japan) and electron microscope (SEM, GAIA3, TESCAN, Germany). Electrospun nanofibers morphology was examined by SEM (Carl Zeiss 300VP, Germany). The diameter of the nanofibers was estimated statistically by taking 100 random readings using ImageJ software.

2.4.2. Zeta potential and size distribution of mBN nanoparticles

Zeta potential and size distribution of the mBN nanoparticles were measured at 25 °C using a Zeta-sizer (Nano-2S-ZEN 3600, Malvern Instruments, Worcestershire, UK). 10 mg of the mBN nanoparticles were dispersed in distilled water (adjusted pH to 7.0 using NaOH) prior to analysis.

2.4.3. Fourier-transform infrared spectroscopy (FTIR)

FTIR was used to evaluate the functional groups of PVA/PAA and mBN-PVA/PAA composite nanofibers using a spectrophotometer (Bruker Vertex 70V). The FTIR spectra were recorded in the range of 40–4000 cm^{-1}.

2.4.4. Contact angle measurements

The wettability performance of the surface of electrospun fibers was assessed by surveying the water contact angle using KSV Attension Theta Lite Optical Tensiometer. A small drop of distilled water was placed onto

the dry sample surface, and the contact angle was recorded at 10 s.

2.4.5. Thermal gravimetric analysis (TGA)

The thermal properties of PVA/PAA and mBN-PVA/PAA nanofibers were determined using TGA (Q600, USA).

2.4.6. Thermal conductivity (TC)

Before TC analysis (Linseis LFA 1000 laser flash), PVA/PAA and mBN-PVA/PAA composite nanofibers were dried in 40 °C vacuum oven until obtained a constant mass and pelleted using 10 kN pressure.

2.4.7. Mechanical test

Tensile properties of PVA/PAA and mBN-PVA/PAA composite nanofiber (20x4 mm) were evaluated using a loading cell of 10 kN displacement rate of 3 mm/min by universal test device (Instron).

2.4.8. Swelling and hydrolytic degradation studies

The water absorption behavior of PVA/PAA and mBN-PVA/PAA composite nanofibers was measured by gravimetric analysis. Dried and pre-weighed samples were immersed in PBS (10 mL, pH 7.4) at room temperature. The swelling degree was calculated as follows;

$$\text{Swelling Degree } (\%) = (W_s\text{-}W_d/W_d) *100 \quad (1)$$

where W_d and W_s are weights of dried and swollen polymers, respectively.

Hydrolytic degradation experiments were performed to determine the stability of nanofibers using the previously described method (Díez-Pascual and Díez-Vicente, 2016). The PVA/PAA and mBN-PVA/PAA nanofibrous mats (1 cm x1 cm) were weighed (Wi) and incubated in PBS solution (pH 7.4, 10 mL) at 37 °C and 100 rpm in shaking water for 3 days. After that, swollen nanofibers were rinsed with deionized water to remove residual buffer salts. And then, samples were dried until constant weight and again weighed (Ws). The degradation ratio was calculated using the following equation:

$$\text{Degradation percentage} = (\text{Wi-Ws/Wi}) * 100 \quad (2)$$

where Wi and Ws are weights of polymer before and after the degradation process, respectively.

2.4.9. In vitro cytocompatibility test

Biocompatibility of PVA/PAA and mBN-PVA/PAA composite nanofibers was evaluated via cytotoxicity method according to ISO 10993–5 (Biological evaluation of medical devices, 2010). For analysis, L929 cells, cultivated in DMEM (Dulbecco's modified Eagle's medium) containing FBS (Fetal bovine serum, 10%), penicillin/streptomycin, and L-glutamine (1%) during 24 h at 37 °C in 5% CO_2-humidified atmosphere, were used. L929 cells (1×10^4 cells/mL) were seeded in 96-well plates containing DMEM and incubated for 24 h at 37 °C. The PVA/PAA and mBN-PVA/PAA composite nanofibers were equally cut and sterilized under UV light for 1 h and incubated in this medium for 24 h, then the metabolic activity of L929 cells was determined using MTT analysis (Erdem et al., 2021; Tevlek et al., 2017).

The activity of mBN-PVA/PAA nanocomposite nanofibers against Human Umbilical Vein Endothelial Cells (HUVEC) was also determined for 72 h *in vitro* conditions. The cells were cultivated in E-plates 16 (16 wells culture dish covered with a gold microelectrode array) using xCELLigence System RTCA DP Instrument from Roch. For this purpose, the cells were grown to ~80% confluence and detached from the flasks by a brief treatment with trypsin/EDTA. 50 μL of cell culture media at room temperature was added into each well of the E-plate. The E-plate was connected to the system and the background impedance was measured. Meanwhile, the cells were resuspended in cell culture medium and added to the wells on the E-plate to obtain a final volume of 100 μL and $5x10^3$ cells/well concentration. Cells were allowed to settle for 30 min at room temperature and then placed into the CO_2 incubator. The software was programmed to take hourly measurement and cells were grown for 24 h. The media was replaced with the respective dilutions of the extracts after 24 h and the measurements were resumed for a further 48 h. The cytolysis rate was calculated on the RTCA-integrated software of the xCELLigence system using the cell index values.

2.4.10. Hemolytic activity

The interaction between PVA/PAA and mBN-PVA/PAA composite nanofibers and red blood cells was determined by hemolysis experiments (2022/05–29). Hemolysis assays were performed according to previously recorded methods in literature (Dey and Ray, 2003; Qu et al., 2006).

2.4.11. Antimicrobial activity

The antibacterial activity of mBN-PVA/PAA composite nanofibers was investigated against*E. coli* ATCC 25922 and *S. aureus* ATCC 25923, according to the American standard test method (ASTM E2149-13a, 2013). Briefly, The mBN-PVA/PAA composite nanofibers were cut into 1 cm x 1 cm and were sterilized under a UV lamp. All samples were added to the liquid bacterial cultures prepared using fresh bacterial strains ($1x10^7$ CFU/mL for *E. coli*, $1x10^5$ CFU/mL for *S. aureus*) in 50 mL phosphate buffer at 37 °C at 150 rpm in a shaking incubator for 24 h. After incubation, an aliquot of the bacterial solution was withdrawn and spread on nutrient agar plates. The bacteria were again cultured on the agar plate for 24 h and the surviving colonies are counted (Arkoun et al., 2017).

3. Result and discussion

3.1. Morphology and structure

In this study, uniform, bead-free, and water-resistant PVA/PAA nanofibers, which form the structural framework for the mBN nanoparticles, were successfully fabricated. Fig. 1 shows the morphology and the size distribution of the mBN nanoparticles. The mBN nanoparticles appear to have spherical geometry and narrow size distribution (Fig. 1a). The dark and bright phases seen in the TEM micrographs are due to the difference in layer thicknesses of the layered boron nitride (W. Wang et al., 2017) (Fig. 1b). The ζ-potential value of mBN nanoparticles was measured as −17.4 mV (at pH 7.0) indicating mBN nanoparticles tend to aggregation at this conditions. The ζ-potential value should be above 30 mV for a stable colloidal system (Tian et al., 2021; Zhao et al., 2019; Zhou et al., 2022). Fig. 1c indicates that 56% of the nanoparticles had a 200–400 nm hydrodynamic radius and an average hydrodynamic radius of 276.5 nm (PDI: 0.255).

The water stability of the mBN-PVA/PAA fibrous scaffolds was achieved by thermal cross-linking between the hydroxyl groups of PVA and the carboxyl groups of PAA. Fig. 2 presents the SEM micrographs of the PVA/PAA hybrid nanofibers with different mBN contents after the thermal treatment. Thermal crosslinking did not cause any notable change in fiber diameters while retaining the fibrous structure of the scaffolds. Similarly, Chee et al. (2021) reported that no statistically significant change was observed in the diameters of unannealed and annealed PVA and PAA nanofibers. Besides, the fact that the thinner nanofibers may behave differently under annealing was associated with exceeding the glass transition temperature of the polymer. Another complementary finding is that, unlike pure PVA or PAA nanofibers, Tg was unaffected in PVA/PAA bilayer nanofibers.

The morphologies of the PVA/PAA nanofibers were regular and a narrow distribution of diameters was observed (222 ± 17 nm). The PVA/PAA nanofibers have a smooth surface (Fig. 2a) indicating that PAA was well dispersed in the PVA solution as a result of the electrospinning conditions using appropriate concentrations. After adding mBN, the composite nanofibers showed similar morphology with PVA/PAA, indicating a significantly interconnected fiber structure (Fig. 2b–e). Furthermore, no agglomeration between both neat PVA/

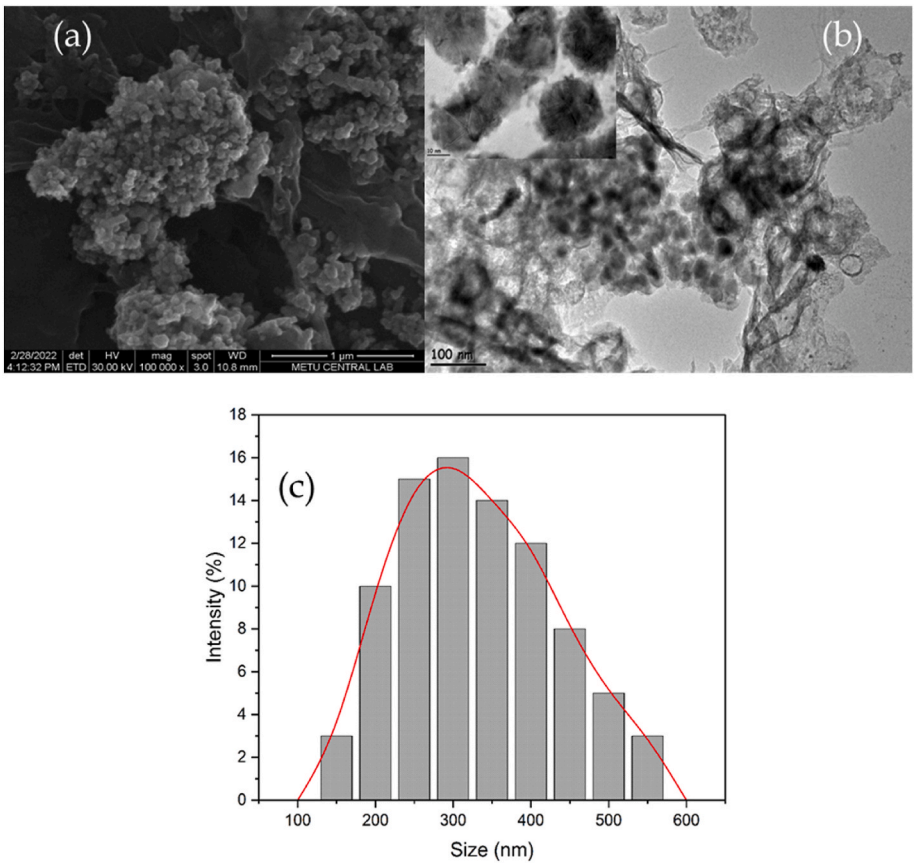

Fig. 1. SEM (a) and TEM (b) micrographs; size-distribution (c) of mBN nanoparticles dispersed in water.

PAA nanofibers and the mBN-PVA/PAA composite nanofibers (0.5, 1.0, and 2.0 wt%) was observed. However, at higher mBN content (5.0 wt%), the aggregates were often observed (Fig. 2e), due to partial aggregations of the mBN. The fiber geometry of the PVA/PAA containing 5.0 wt% mBN started to deteriorate may be due to an excessive increase in polymer viscosity.

As also seen from EDS spectra, neat PVA/PAA fiber and all mBN-PVA/PAA composite fibers have C and O peaks. The mBN incorporated-fibers have also B and N peaks at higher mBN content. A slight increase in the average fiber diameter of the mBN-PVA/PAA composite nanofibers was observed as increasing the mBN contents may be attributed to an increase in the viscosity of the blend solution (Fig. 3). While the average fiber diameter of mBN0.5-PVA/PAA composite nanofiber was 305 ± 15 nm, it was 281 ± 11 nm at 5 wt% mBN. Furthermore, the interaction between the hydroxyl or carboxyl groups of the polymer and the mBN surface limited the mobility of the polymer chains. The fiber diameter increased as the greater viscoelastic force prevented axial strain during the whipping process (Kim et al., 2019). Another effect of mBN with its high thermal conductivity coefficient is thought to contribute extra to the axial orientation of the polymer chains during electrospinning (Z. Wang et al., 2018).

The water contact angle is the simplest method to measure the wettability of solid surfaces. As the hydrophilicity of the surface increases, the contact angle with water decreases (Chee et al., 2021). The change in hydrophilicity of mBN-PVA/PAA composite nanofibers was evaluated using a water contact angle. Fig. 4 shows that the surface wettability of PVA/PAA nanofibers was better than mBN-PVA/PAA composite nanofibers. In addition, the contact angle of the PVA/PAA surface (20.762° ± 1.44) increased compared to the mBN-PVA/PAA surface as a function of mBN content indicating a decrease in hydrophilicity. The contact angle of mBN0.5-PVA/PAA, mBN1-PVA/PAA, mBN2-PVA/PAA, and mBN5-PVA/PAA composite nanofibers was 25.027° ± 2.32, 35.091° ± 2.12, 33.330° ± 1.55, and 45.249° ± 1.21, respectively.

The increased water stability of mBN-PVA/PAA composite nanofibers may be due to the increase in the average diameter of the nanofibers after adding mBN (Fig. 3). It may also result from the formation of hydrophobic ester groups between PVA and PAA molecules during thermal/physical crosslinking of PVA chains with each other, and with hydroxylated-BN nanoparticles (Chee et al., 2021; Kumeta et al., 2003; Lim et al., 2016; Zeng et al., 2004).

The FTIR spectra were used to characterize interactions between PVA, PAA, and mBN which are components of composite nanofiber (Fig. 5). As expected FTIR spectrum of PVA/PAA nanofibers exhibited typical absorption bands at 1092 cm^{-1}, 1266 cm^{-1}, 1438 cm^{-1}, 1714 cm^{-1}, 2915 cm^{-1}, and 3350 cm^{-1} which can be attributed to the C–O–C stretching, C–O stretching, C–H bending, C═O stretching, CH_2 stretching vibrations and the stretching vibration peak of O–H groups, respectively (Chee et al., 2021; Kim et al., 2018; Lee et al., 2012). After insertion of mBN into the PVA/PAA nanofiber, two specific BN vibration peaks were observed at around 800 cm^{-1} and 1390 cm^{-1} corresponding to the in-plane B–N and B–N–B stretching vibrations, and out-of-plane bending vibrations, respectively (Konyashin et al., 1997; Shapoval et al., 1990; Sun and Bi, 2021; Xie et al., 2020; Ye et al., 2019).

As previously reported that an esterification reaction occurred with the presence of –OH groups of PVA and –COOH groups of PAA. It can be indicated by the observation of the peaks at 1714 cm^{-1} (C═O stretching) and 1255 cm^{-1} (C–O–C stretching). The intensity of C═O is reduced depending on mBN content due to the restriction of PVA and PAA chains, especially at high mBN content. On the other hand, the intensity of characteristic peaks of BN increased depending on mBN content observed at around 800 cm^{-1}, and 1390 cm^{-1}.

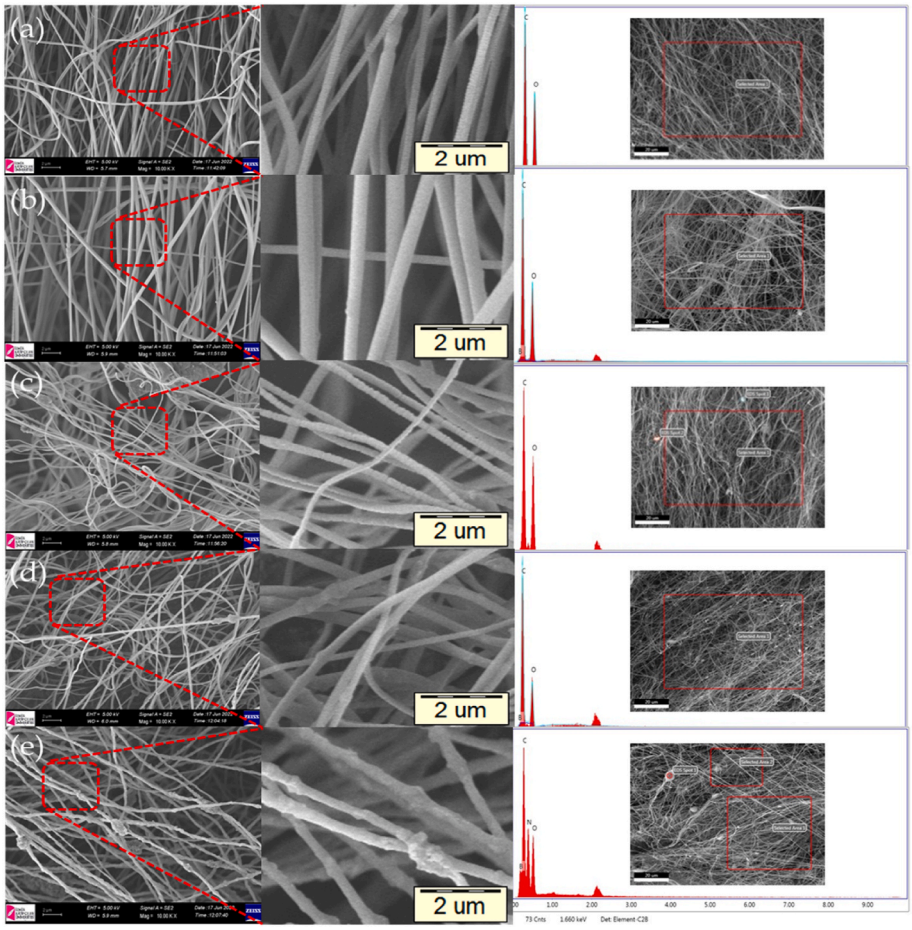

Fig. 2. SEM micrographs and EDS spectra of nanofibers: neat PVA/PAA (a); mBN-PVA/PAA composites with 0.5 wt% (b), 1 wt% (c), 2 wt% (d), 5 wt%(e). Middle images show a small area of the micrographs at higher magnification.

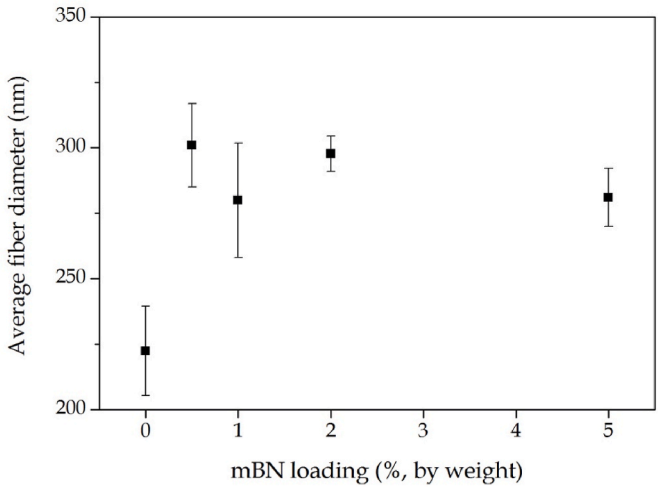

Fig. 3. Variation of average fiber diameter with mBN content.

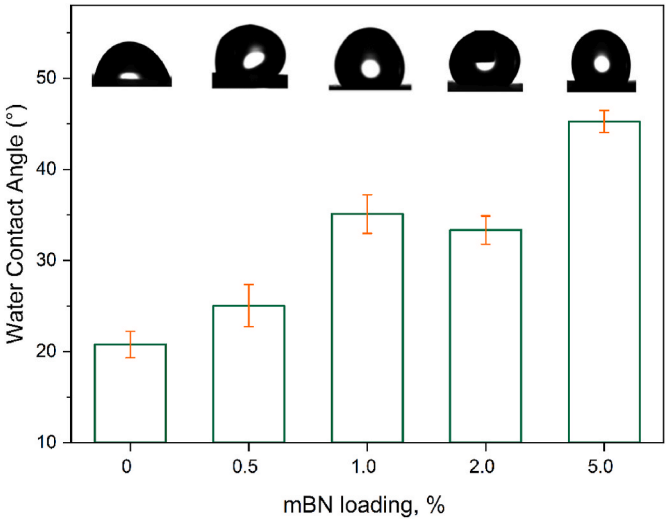

Fig. 4. Images of the water droplets on composite nanofibers and contact angle measurements.

3.2. Thermal stability

Fig. 6 shows the thermal degradation curves of PVA/PAA-based composite nanofibers in the range of 25–600 °C. It has been previously reported that BN has a thermally stable structure without any weight loss up to 800 °C (Duan et al., 2013). However, all composite nanofibers have three thermal degradation steps. At 10% weight loss ($T_{10\%}$), the thermal decomposition temperature of mBN-PVA/PAA composite nanofibers increases by 33 °C compared to that of PVA/-PAA nanofibers. The significantly improved thermal stability is due to the BN nanolayers uniformly dispersed between the PVA/PAA chains (Duan et al., 2013). After adding mBN, the temperatures in the region

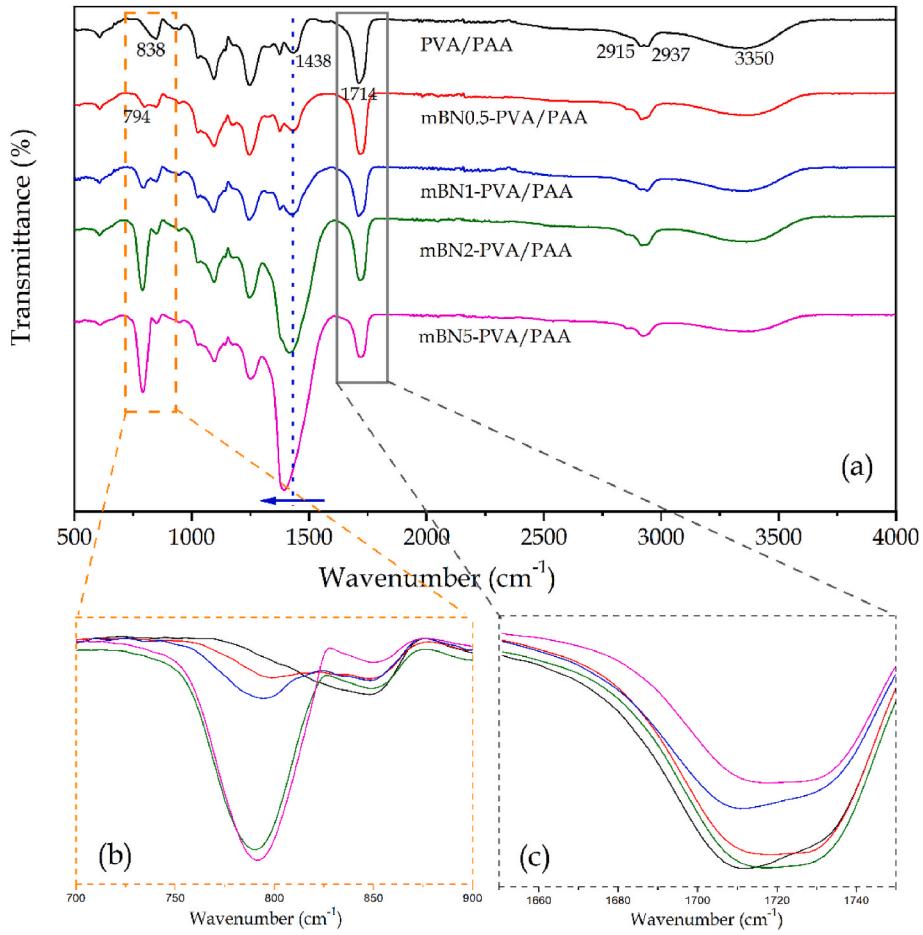

Fig. 5. FTIR results of the PVA/PAA-based composite nanofibers (a) enlargements of the wavenumber range 700–900 cm^{-1} (b) and 1650–1750 cm^{-1} (c).

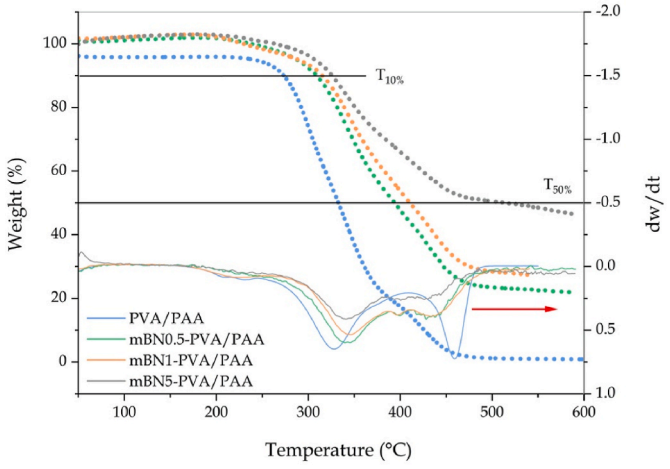

Fig. 6. TG and DTG curves of mBN-PVA/PAA composite nanofibers.

where the maximum loss occurred (between 350 °C and 500 °C) shifted to higher temperatures, indicating the enhancement in thermostability. Furthermore, the increase in thermal stability was supported by the temperature at which 50% weight loss occurred ($T_{50\%}$) and the increase in the % residue amount (m_{dec},%) at 600 °C was higher than those of PVA/PAA nanofibers (Table 1).

The significant increase in thermal stability can be affected by not only the excellent thermal stability of BN but also the orientation of the composite fibers (Chen et al., 2019). It is reported that the BN nanolayers between polymer chains may act as a physical barrier, delaying the escape of decomposition products and causing the thermal decomposition temperature to shift towards higher temperatures (Chen et al., 2019). Thus, the thermal stability of the composite nanofibers was greatly improved.

The mass losses of PVA/PAA and mBN-PVA/PAA composite nanofibers in the temperature range of 200–500 °C (the step with the highest mass loss for all samples), and the kinetic parameters calculated using the Coats-Redfern equation (Al-Shemy et al., 2022) are given in Table 1. The change in the activation energies of the samples follows this order: PVA/PAA < mBN0.5-PVA/PAA < mBN1-PVA/PAA < mBN2-PVA/PAA

Table 1
Thermodynamic parameters of mBN reinforced PVA/PAA composite nanofibers (200 °C–450 °C).

Material	$T_{10\%}$	$T_{50\%}$	m_{dec}%	Ea (kJ/mol)	ΔH (kJ/mol)	ΔG (kJ/mol)	ΔS (kJ/mol K)	A (s^{-1})
PVA/PAA	292.7	332.8	0.681	16.85	12.92–10.84	127.85–188.71	−0.243-(-0.246)	2.058
mBN0.5-PVA/PAA	308.7	393.8	21.87	26.58	22.65–20.56	127.66–183.96	−0.222-(-0.226)	22.57
mBN1-PVA/PAA	315.3	410.2	27.51	49.09	45.15–43.08	131.85–178.83	−0.183-(-0.188)	2351.4
mBN2-PVA/PAA	299.2	476.8	34.01	43.24	39.31–37.32	135.80–187.61	−0.204-(-0.208)	205.29
mBN5-PVA/PAA	325.8	513.3	46.40	50.18	46.25–44.19	131.39–177.22	−0.180-(-0.184)	3748.8

< mBN5-PVA/PAA. The increase in activation energy is thought to be caused by the cross-linking effect of hydroxylated-BN with both PVA and PAA (increase in thermal stability). Moreover, the activation enthalpy (ΔH) and Gibbs free energy (ΔG) follow the same order as activation energy (Al-Shemy et al., 2022). In contrast, activation entropies (ΔS) decreased with incorporation of mBN. The enthalpy, which indicates the heat content in a system, changes when energy is absorbed or released at constant pressure (Al-Shemy et al., 2022; Naqvi et al., 2019; Raza et al., 2022). Positive ΔH values indicate endothermic systems, while negative values are for exothermic reactions. The calculated ΔH values for all nanofiber samples are positive, indicating that energy is needed for decomposition (Naqvi et al., 2019; Raza et al., 2022). The change in Gibbs free energy gives information about reaction energy and spontaneity (Naqvi et al., 2019; Raza et al., 2022). Positive ΔG values indicate that energy is needed to start the reaction. Negative ΔS values indicate that the products are less disordered due to bond breaking than the initial conditions (Naqvi et al., 2019; Raza et al., 2022). That is, it shows that the products in the decomposed state have a more ordered structure than before the thermal decomposition, which may be due to the hydroxylated-BN nanolayers between the polymer chains still making interactions such as hydrogen bonds between the degraded polymer chains.

3.3. Thermal conductivity

The thermal conductivities were measured to investigate further the influence of mBN on the thermal conduction property of the composite nanofiber (Fig. 7). Meanwhile, as expected, the thermal conductivities of composite nanofiber increased compared to that of PVA/PAA nanofiber, indicating that adding mBN further accelerates the thermal response of PVA/PAA (Yin et al., 2019). The concentration of mBN in PVA/PAA nanofibers dramatically affects the number of heat conduction paths (Feng et al., 2021). Nevertheless, when the content of mBN exceeds 1.0 wt%, the thermal conductivity of composite nanofibers begins to decrease slightly may be due to the deformation of the polymer structure as a result of the aggregation of mBN. Thus, gaps formed in the heat transfer paths cause a slight repetitive decrease in thermal conductivity.

3.4. Mechanical properties

Mechanical features of mBN-PVA/PAA nanofibers such as tensile strength, elongation at break, and modulus of elasticity were evaluated.

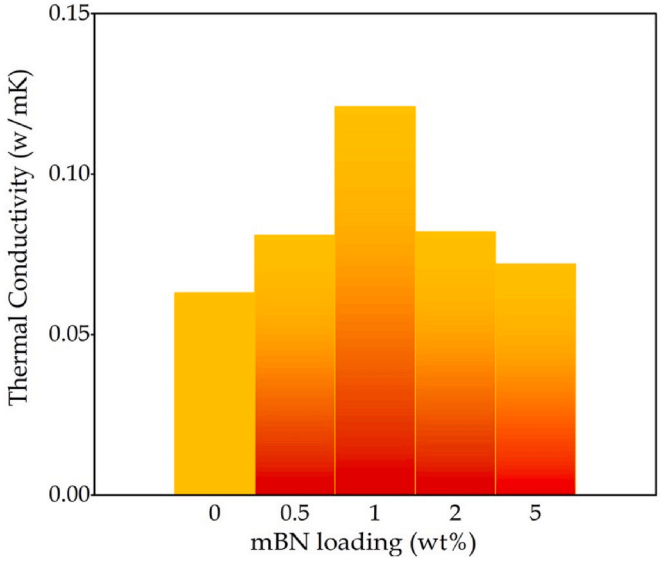

Fig. 7. Thermal conductivity of PVA/PAA-based composite nanofibers.

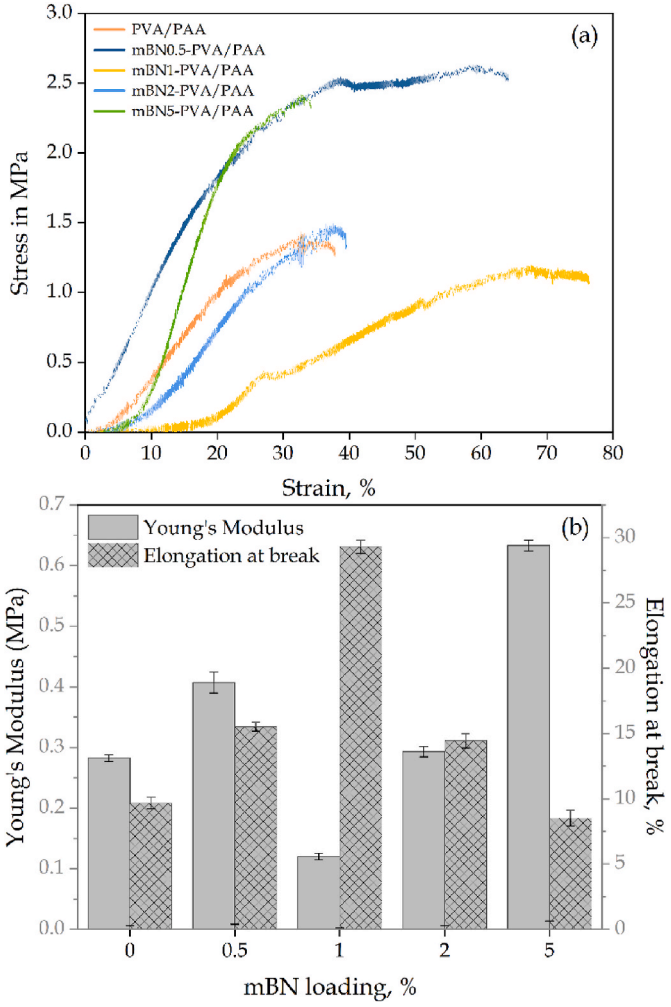

Fig. 8. Mechanical performance of PVA/PAA and mBN-PVA/PAA nanofiber as a function mBN content under tensile stress: (a) tensile strength, (b) Young's modulus and elongation at break (Loading speed: 3 mm/min).

Fig. 8a shows the strain-stress curves of mBN-PVA/PAA composite nanofiber with different loading amounts of mBN. Tensile strength of mBN-incorporated PVA/PAA nanofibers exhibited a nonlinear and discontinuous increment as a function of mBN. The tensile strength and the elongation values at break increased when compared with PVA/PAA nanofibers until 2 wt% mBN loading and then decreased again (Fig. 8b). Similarly, elastic modulus exhibited discontinuous alteration compared with PVA/PAA. At the lowest mBN loading due to the increase in fiber diameter, elastic modulus increased then decreased and reached maximum value at 5 wt% mBN loading. The values of elastic modulus of PVA/PAA, mBN0.5-PVA/PAA, mBN1-PVA/PAA, mBN2-PVA/PAA, and mBN5-PVA/PAA were 0.282 MPa, 0.407 MPa, 0.123 MPa, 0.293 MPa, and 0.633 MPa, respectively (Fig. 8b). The alteration in values of the elastic modulus, elongation at break, and tensile strength may be due to change in average fiber diameter (Fig. 3) or increment of hydrogen bonds formed between polymer chains and the hydroxylated-BN at high concentrations. It also may be said that the rise of the volumetric ratio of mBN in the composite effects the orientation of the fiber by affecting the surface energy and thus increasing the tensile strength. The mBN loading exhibits a higher mechanical enhancement effect towards PVA/PAA nanofiber due to the two-dimensional structure of BN; mechanical load can be easily transferred to BN, indicating that the mBN could be used as an effective reinforcing agent for PVA/PAA nanofiber by adjusting the loading amount according to the targeted application (Weng et al., 2016; Yin et al., 2019).

3.5. Swelling behavior and weight loss study

The alteration of swelling behavior of PVA/PAA and mBN-PVA/PAA composite nanofibers as a function of time was shown in Fig. 9a. As seen, the swelling rate of all nanofibers was very fast, the neat PVA/PAA nanofiber has achieved full swelling in 2 min, then swelling rate started to decrease due to the disintegration of nanofibers and reached the plateau in 60 min. Adding mBN affected the maximum swelling capacity and time to reach an equilibrium of PVA/PAA nanofibers. Although the maximum swelling capacity of the samples containing mBN0.5 and mBN1 is lower than PVA/PAA, their equilibrium swelling capacity is higher than PVA/PAA since they maintain stability for a longer time. It can be attributed to the hydrogen bonding of hydroxylated BN with both PVA/PAA and water molecules. The maximum swelling values of mBN2-PVA/PAA and mBN5-PVA/PAA composite nanofibers were decreased compared to PVA/PAA, mBN0.5-PVA/PAA, and mBN1-PVA/PAA. This decrease observed in the swelling values of nanofibers containing high concentrations of mBN may be due to the increase in the number of hydrogen bonds formed with the increase of mBN, consequently, the increase in crosslinking density, which reduces the free volume in the polymer network (Chee et al., 2021).

The percentage of weight loss of PVA/PAA, mBN0.5-PVA/PAA, mBN1-PVA/PAA, mBN2-PVA/PAA, and mBN5-PVA/PAA composite nanofiber at 60 min was 8.0%, 7.84%, 6.12%, 7.69%, and 5.81%, respectively. Concerning time and amount of mBN increased, percent weight loss increased and reached 26.86%, 22.08%, 14.73%, 12.74% and 11.03%, respectively (Fig. 9b). The water stability of PVA/PAA nanofiber was improved by adding mBN. According to both swelling and degradation properties, the addition of mBN can be controlled the swelling and degradation process enabling the improvement of the drug release profile of PVA/PAA nanofiber.

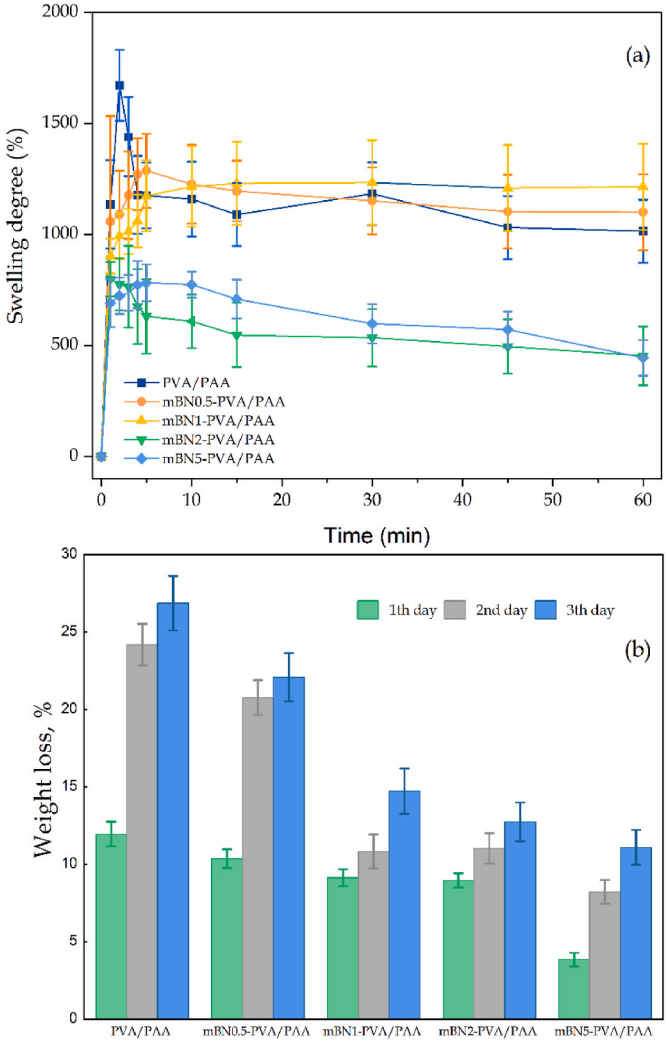

Fig. 9. (a) Swelling and (b) degradation characteristics of PVA/PAA-based composite nanofibers.

3.6. In vitro biocompatibility

Materials are called nontoxic when cell viability changesd in the range of 75%–100% according to ISO 10993–5:2009 (E) (He et al., 2013; Li et al., 2020; Xi et al., 2009). The cytotoxicity of the mBN-PVA/PAA composite nanofibers was first evaluated using L929 cell lines. Fig. 10a presents the viability of L929 cells after 24 h in contact with PVA/PAA and mBN-PVA/PAA composite fibers. While the viability of cells in contact with PVA/PAA was around 89.74 ± 0.77%, it was slightly changed by adding mBN. The cell viability in mBN0.5-PVA/PAA, mBN1-PVA/PAA, mBN2-PVA/PAA, and mBN5-PVA/PAA composite nanofibers was 91.94 ± 1.85%, 93.2 ± 2.08%, 94.3 ± 2.35%, and 90.5 ± 1.25%, respectively. The mBN addition to PVA/PAA nanofibrous membranes did not significantly influence the growth of L929 cells and we can say that all composite nanofibers have non-toxicity (cell viability >75%). Several studies have reported that the toxicity of BN depends on various parameters such as size, concentration, synthesis process, surface modification, and cell type (Díez-Pascual and Díez-Vicente, 2016). It is remarked that hBN nanoparticles had non-toxicity for both CRL 2120 cells and MDCK cells at low concentrations (0.025, 0.05, 0.1 mg/mL)(Kıvanç et al., 2018). In another study, BN nanotubes have caused inconsiderable toxicity for fibroblast cells at high concentrations (≥50 mg/mL) (Ferreira et al., 2011). These data demonstrate the biocompatibility of the composite nanofibrous materials and their suitability as biomaterials such as wound healing or drug delivery vehicles.

After MTT analysis of composite nanofibers, the effect on cell viability was investigated in real-time with HUVEC cells with the Xcellienge cell analysis system. After 24 h, the composite nanofibers showed similar properties with the control group until the 48th hour which can be explained why the composite electrospun nanofibers did not seem to have any cellular toxicity effects on HUVEC cell lines (Gholami et al., 2018), and there was no adverse effect on cell cytolysis after 48 h, and it was within acceptable limits, illustrated in Fig. 10b.

3.7. Hemolytic activity

In conjunction with cytotoxicity analysis, the effect of mBN-PVA/PAA electrospun nanofibers on red blood cells (RBCs) was evaluated to verify biological safety, and that it is harmless to the body as a biomedical wounding dressing (Zhou et al., 2022) (Fig. 11). The percentage of hemolysis of PVA/PAA, mBN0.5-PVA/PAA, mBN1-PVA/PAA, mBN2-PVA/PAA, and mBN5-PVA/PAA composite nanofibers were calculated as 1.839 ± 0.016, 1.913 ± 0.03, 1.692 ± 0.013, 1.839 ± 0.03, and 1.618 ± 0.013%, respectively (Fig. 11a). Hemolytic activity of all electrospun nanocomposite fibers was less than 5% (clinical biomedical application standard) (Zhou et al., 2022), indicating designed composite nanofibers have an acceptable value for biomaterials (Geng et al., 2016; Haghniaz et al., 2021; X. Xie et al., 2021) and hemolysis of neat PVA/PAA has mostly stayed the same with the incorporation of mBN. However, the colors of the supernatant after the hemolysis test of both PVA/PAA and mBN-PVA/PAA were transparent and slightly yellow at the highest nanofiber concentration (Fig. 11b). The effect of PVA/PAA and mBN-PVA/PAA concentration interacting with RBCs was investigated in the range of 60–240 μg/mL. The composite nanofiber concentration in this range did not adversely affect the percent of hemolysis. The hemolytic activity of PVA/PAA at 60 μg/mL was 1.25%, while it was 1.83% at 240 μg/mL. However, the percentage

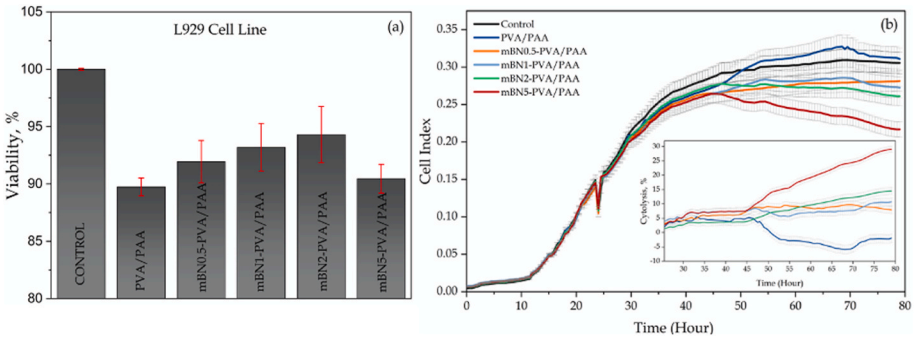

Fig. 10. Cytotoxicity of mBN-PVA/PAA composite electrospun nanofibers against to L929 Fibroblast cell line (a) and HUVEC cell line in real-time (b).

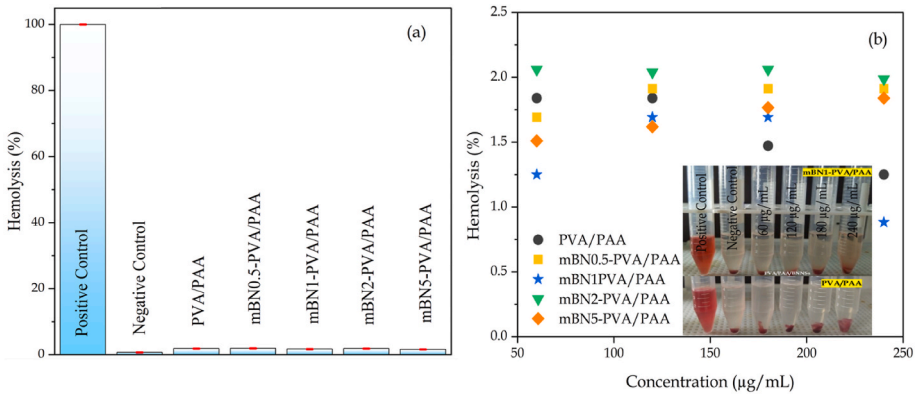

Fig. 11. Hemolysis percentage of the composite nanofibers at 180 µg/mL (a) Effect of composite nanofiber concentration on hemolysis percentage (60–240 µg/mL) and pictures from hemolysis assays of the PVA/PAA and mBN1-PVA/PAA composite nanofibers (b).

of hemolysis of mBN0.5-PVA/PAA, mBN1-PVA/PAA, mBN2-PVA/PAA, and mBN5-PVA/PAA was determined as 1.69%, 1.25%, 2.06%, and 1.83% at 240 µg/mL indicating the composite nanofibers can be safely used according to clinical biomedical application standard. According to the hemolytic activity results, mBN incorporation in PVA/PAA nanofibers has not negatively changed of hemocompatibility and it could be used as a biomaterial for various biomedical applications.

3.8. Antimicrobial activity

Investigation of antibacterial activity of newly-purposed biomaterials is an important issue due to microorganisms which are usually *E. coli* (as gram-negative bacteria) and *S. aureus* (gram-positive bacteria) can cause infections in/on biomaterials (Díez-Pascual and Díez-Vicente, 2016). For this purpose, the antibacterial activity of mBN-PVA/PAA composite electrospun nanofibers was tested using *E. coli* and *S. aureus*, and the antibacterial rate (AR) of each electrospun nanofiber composite was calculated as follows:

$$AR\ (\%) = (N_o\text{-}N_s/N_o)*100 \quad (4)$$

where N_o is the number of colonies corresponding to the control group, and N_s is the number of colonies corresponding to the electrospun nanocomposite.

As seen, compared with the control, the antibacterial activity increased with mBN content after 24 h incubation (Fig. 12). The difference was higher for the reduction in the number of colonies of *S. aureus* than for *E. coli*. The percentage reduction (calculated as AR%) was 65% and 75% for *E. coli* and *S. aureus*, respectively. The difference in the antibacterial behavior of electrospun composite nanofibers can be related to the structure of cell walls (Deshmukh et al., 2020; Díez-Pascual et al., 2014). On the other hand, the difference between the two bacterial strains may also be due to the tendency of *S. aureus* to form cellular aggregates rather than its response to surface hydrophilicity (Karakeçili and Gümüşderelioğlu, 2002; Santiago-Morales et al., 2016). Although, the certain physical or chemical mechanism of the bacteriocidal effect of BN has not been completeley explained (Díez-Pascual and Díez-Vicente, 2016; Doğan and Metin, 2022; Pandit et al., 2019), the potential mechanisms for the antibacterial activity of BN-based materials could be oxidative stress from the generation of reactive oxygen species (Díez-Pascual and Díez-Vicente, 2016; Kalay et al., 2015), membrane damage from the insertion of BN nanomaterials into the cell membrane (Díez-Pascual and Díez-Vicente, 2016; Thomas et al., 2015), and the ability to perform endocytosis (Díez-Pascual and Díez-Vicente, 2016; Horváth et al., 2011). Similar results on the antimicrobial effect of BN nanoparticles in which polymer composites have been reported (Deshmukh et al., 2020; Doğan and Metin, 2022; Kıvanç et al., 2018; Pandit et al., 2019; Yegin et al., 2022). Yeğin et al. showed that PNMP-BN composite had antibacterial activity against *E. coli*, *S. aureus*, *P. aeruginosa*, and *E. faecalis* compared with PNMPy due to effect of van der Waals forces between the layers of h-BN and the lone electron pairs of nitrogen atoms of the BN may make an electrostatic interaction with the cell walls (Ikram et al., 2020; Yegin et al., 2022).

4. Conclusions

This study focused on the fabrication and characterization of mBN-PVA/PAA composite nanofibers. BN was exfoliated by ultrasonication and obtained hydroxlated-BN nanoparticles. FTIR and SEM/EDS results of mBN-PVA/PAA confirmed that hydroxylated-BN was well dispersed in the polymer matrix. The mBN-PVA/PAA composite nanofibers showed high thermal stability and durability compared to PVA/PAA. Mechanical properties and thermal conductivities of nanofibers improved depending on the mBN loading in the composite nanofibers. Remarkably improved elastic modulus of PVA/PAA with mBN loading at

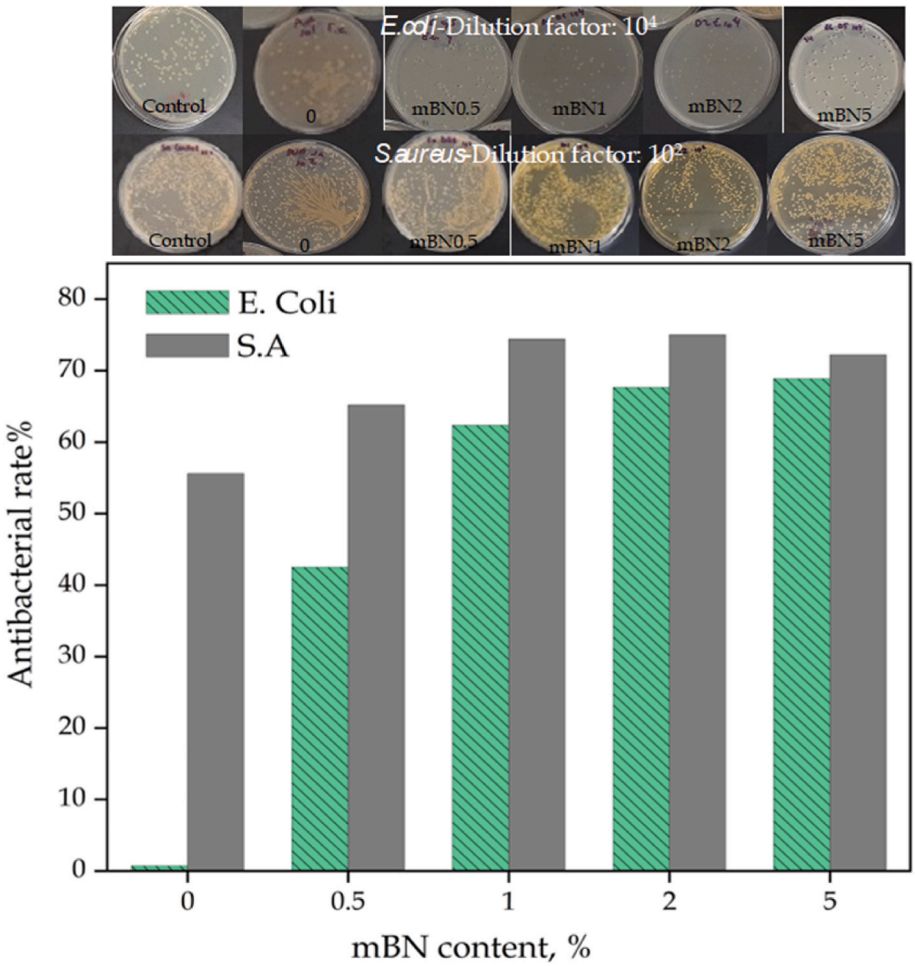

Fig. 12. Antimicrobial rate of mBN-PVA/PAA composite fibers.

5 wt% may be reached an opinion that it has a potential to produce soft electronics used for monitoring various movements (e.g. facial or arthrosis movements). Also, swelling profile of the PVA/PAA nanofiber was controlled by adding mBN, and the wettability of mBN-PVA/PAA composite nanofibers decreased indicating a rise of hydrophobicity in PVA/PAA. The hydrophilic/hydrophobic composition of mBN-PVA/PAA may provide a synergistic effect on dual drug delivery systems. The MTT assay confirmed the non-toxicity of mBN-PVA/PAA for the L929 cell line and HUVEC cell line in real-time, and they could inhibit bacterial growth. The findings of this study may open new doors using PVA/PAA nanofibers as a biomaterial for a wide range of biological applications, especially drug delivery systems, soft materials, or wound healing.

CRediT authorship contribution statement

Deniz Doğan: Visualization, Validation, Investigation. **F. Rabia Karaduman:** Methodology, Investigation. **Nesrin Horzum:** Writing – review & editing, Supervision, Project administration, Methodology, Conceptualization. **Ayşegül Ülkü Metin:** Writing – review & editing, Writing – original draft, Supervision, Project administration, Methodology, Conceptualization.

Declaration of competing interest

The authors declare that they have no known competing financial interests or personal relationships that could have appeared to influence the work reported in this paper.

Data availability

Data will be made available on request.

References

Al-Dhahebi, A.M., Gopinath, S.C.B., Saheed, M.S.M., 2020. Graphene impregnated electrospun nanofiber sensing materials: a comprehensive overview on bridging laboratory set-up to industry. Nano Converg. https://doi.org/10.1186/s40580-020-00237-4.

Al-Shemy, M.T., Al-Sayed, A., Dacrory, S., 2022. Fabrication of sodium alginate/graphene oxide/nanocrystalline cellulose scaffold for methylene blue adsorption: kinetics and thermodynamics study. Sep. Purif. Technol. 290 https://doi.org/10.1016/j.seppur.2022.120825.

Alva, G., Lin, Y., Fang, G., 2018. Thermal and electrical characterization of polymer/ceramic composites with polyvinyl butyral matrix. Mater. Chem. Phys. 205, 401–415. https://doi.org/10.1016/j.matchemphys.2017.11.046.

Ambekar, R.S., Kandasubramanian, B., 2019. Advancements in nanofibers for wound dressing: a review. Eur. Polym. J. https://doi.org/10.1016/j.eurpolymj.2019.05.020.

Arafat, M.T., Mahmud, M.M., Wong, S.Y., Li, X., 2021. PVA/PAA based electrospun nanofibers with pH-responsive color change using bromothymol blue and on-demand ciprofloxacin release properties. J. Drug Deliv. Sci. Technol. 61 https://doi.org/10.1016/j.jddst.2020.102297.

Arik, N., Inan, A., Ibis, F., Demirci, E.A., Karaman, O., Ercan, U.K., Horzum, N., 2019. Modification of electrospun PVA/PAA scaffolds by cold atmospheric plasma: alignment, antibacterial activity, and biocompatibility. Polym. Bull. 76, 797–812. https://doi.org/10.1007/s00289-018-2409-8.

Arkoun, M., Daigle, F., Heuzey, M.C., Ajji, A., 2017. Antibacterial electrospun chitosan-based nanofibers: a bacterial membrane perforator. Food Sci. Nutr. 5, 865–874. https://doi.org/10.1002/fsn3.468.

ASTM International. ASTM E2149, 2013. Standard Test Method for Determining the Antimicrobial Activity of Antimicrobial Agents under Dynamic Contact Conditions (West Conshohocken, Pennsylvania).

Bao, Q., Zhang, H., Yang, J.X., Wang, S., Tang, D.Y., Jose, R., Ramakrishna, S., Lim, C.T., Loh, K.P., 2010. Graphene-polymer nanofiber membrane for ultrafast photonics. Adv. Funct. Mater. 20, 782–791. https://doi.org/10.1002/adfm.200901658.

Bhardwaj, N., Kundu, S.C., 2010. Electrospinning: a fascinating fiber fabrication technique. Biotechnol. Adv. https://doi.org/10.1016/j.biotechadv.2010.01.004.

Biological evaluation of medical devices-Part 13: Identification and quantification of degradation products from polymeric medical devices Évaluation biologique des dispositifs médicaux-Partie 13: Identification et quantification de produits de dégradation de dispositifs médicaux à base de polymères Copyright International Organization for Standardization Provided by IHS under license with ISO Not for Resale No reproduction or networking permitted without license from IHS, 2010.

Chee, B.S., de Lima, G.G., de Lima, T.A.M., Seba, V., Lemarquis, C., Pereira, B.L., Bandeira, M., Cao, Z., Nugent, M., 2021. Effect of thermal annealing on a bilayer polyvinyl alcohol/polyacrylic acid electrospun hydrogel nanofibres loaded with doxorubicin and clarithromycin for a synergism effect against osteosarcoma cells. Mater. Today Chem. 22 https://doi.org/10.1016/j.mtchem.2021.100549.

Chen, L., Xiao, C., Tang, Y., Zhang, X., Zheng, K., Tian, X., 2019. Preparation and properties of boron nitride nanosheets/cellulose nanofiber shear-oriented films with high thermal conductivity. Ceram. Int. 45, 12965–12974. https://doi.org/10.1016/j.ceramint.2019.03.224.

Deshmukh, A.R., Aloui, H., Kim, B.S., 2020. In situ growth of gold and silver nanoparticles onto phyto-functionalized boron nitride nanosheets: catalytic, peroxidase mimicking, and antimicrobial activity. J. Clean. Prod. 270 https://doi.org/10.1016/j.jclepro.2020.122339.

Dey, R.K., Ray, A.R., 2003. Synthesis, characterization, and blood compatibility of polyamidoamines copolymers. Biomaterials 24, 2985–2993. https://doi.org/10.1016/S0142-9612(03)00122-4.

Díez-Pascual, A.M., Díez-Vicente, A.L., 2016. PEGylated boron nitride nanotube-reinforced poly(propylene fumarate) nanocomposite biomaterials. RSC Adv. 6, 79507–79519. https://doi.org/10.1039/c6ra09884c.

Díez-Pascual, A.M., Xu, C., Luque, R., 2014. Development and characterization of novel poly(ether ether ketone)/ZnO bionanocomposites. J. Mater. Chem. B 2, 3065–3078. https://doi.org/10.1039/c3tb21800g.

Doğan, D., Metin, A.Ü., 2022. Physicochemical and biological assessment of boron nitride nanosheets-reinforced poly(2-hydroxyethylmethacrylate) composite for biomedical applications. Mater. Today Commun., 104807 https://doi.org/10.1016/j.mtcomm.2022.104807.

Duan, Z.Q., Liu, Y.T., Xie, X.M., Ye, X.Y., 2013. A simple and green route to transparent boron nitride/PVA nanocomposites with significantly improved mechanical and thermal properties. Chin. Chem. Lett. 24, 17–19. https://doi.org/10.1016/j.cclet.2012.12.014.

Erdem, U., Bozer, B.M., Turkoz, M.B., Metin, A.U., Yıldırım, G., Turk, M., Nezir, S., 2021. Spectral analysis and biological activity assessment of silver doped hydroxyapatite. Journal of Asian Ceramic Societies 9, 1524–1545. https://doi.org/10.1080/21870764.2021.1989749.

Feng, M., Pan, Y., Zhang, M., Gao, Q., Liu, C., Shen, C., Liu, X., 2021. Largely improved thermal conductivity of HDPE composites by building a 3D hybrid fillers network. Compos. Sci. Technol. 206 https://doi.org/10.1016/j.compscitech.2021.108666.

Ferreira, T.H., Silva, P.R.O., Santos, R.G., Sousa, E.M.B., 2011. A novel synthesis route to produce boron nitride nanotubes for bioapplications. J. Biomaterials Nanobiotechnol. 426–434. https://doi.org/10.4236/jbnb.2011.24052, 02.

Ge, X., Wu, S., Shen, W., Chen, L., Zheng, Y., Ao, F., Ning, Y., Mao, Y., Chen, Z., 2022. Preparation of polyvinylidene fluoride–gold nanoparticles electrospinning nanofiber membranes. Bioengineering 9. https://doi.org/10.3390/bioengineering9040130.

Geng, H., Dai, J., Li, J., Di, Z., Liu, X., 2016. Antibacterial ability and hemocompatibility of graphene functionalized germanium. Sci. Rep. 6 https://doi.org/10.1038/srep37474.

Gholami, L., Kazemi Oskuee, R., Tafaghodi, M., Ramezani Farkhani, A., Darroudi, M., 2018. Green facile synthesis of low-toxic superparamagnetic iron oxide nanoparticles (SPIONs) and their cytotoxicity effects toward Neuro2A and HUVEC cell lines. Ceram. Int. 44, 9263–9268. https://doi.org/10.1016/j.ceramint.2018.02.137.

Golberg, D., Bando, Y., Huang, Y., Terao, T., Mitome, M., Tang, C., Zhi, C., 2010. Boron nitride nanotubes and nanosheets. ACS Nano. https://doi.org/10.1021/nn1006495.

Gonzalez-Ortiz, D., Salameh, C., Bechelany, M., Miele, P., 2020. Nanostructured boron nitride–based materials: synthesis and applications. Mater Today Adv. https://doi.org/10.1016/j.mtadv.2020.100107.

Gu, J., Lv, Z., Wu, Y., Guo, Y., Tian, L., Qiu, H., Li, W., Zhang, Q., 2017. Dielectric thermally conductive boron nitride/polyimide composites with outstanding thermal stabilities via in-situ polymerization-electrospinning-hot press method. Compos Part A Appl Sci Manuf 94, 209–216. https://doi.org/10.1016/j.compositesa.2016.12.014.

Haghniaz, R., Rabbani, A., Vajhadin, F., Khan, T., Kousar, R., Khan, A.R., Montazerian, H., Iqbal, J., Libanori, A., Kim, H.J., Wahid, F., 2021. Anti-bacterial and wound healing-promoting effects of zinc ferrite nanoparticles. J. Nanobiotechnol. 19 https://doi.org/10.1186/s12951-021-00776-w.

He, L., Lei, W., Liu, D., 2021. One-step facile fabrication of mechanical strong porous boron nitride nanosheets–polymer electrospun nanofibrous membranes for repeatable emulsified oil/water separation. Sep. Purif. Technol. 264 https://doi.org/10.1016/j.seppur.2021.118446.

He, Y., Wang, W.R., Ding, J.D., 2013. Effects of L-lactic acid and D,L-lactic acid on viability and osteogenic differentiation of mesenchymal stem cells. Chin. Sci. Bull. 58, 2404–2411. https://doi.org/10.1007/s11434-013-5798-y.

Hejabri Kandeh, S., Amini, S., Ebrahimzadeh, H., 2021. Simultaneous trace-level monitoring of seven opioid analgesic drugs in biological samples by pipette-tip micro solid phase extraction based on PVA-PAA/CNT-CNC composite nanofibers followed by HPLC-UV analysis. Microchim. Acta 188. https://doi.org/10.1007/s00604-021-04931-w.

Horváth, L., Magrez, A., Golberg, D., Zhi, C., Bando, Y., Smajda, R., Horváth, E., Forró, L., Schwaller, B., 2011. In vitro investigation of the cellular toxicity of boron nitride nanotubes. ACS Nano 5, 3800–3810. https://doi.org/10.1021/nn200139h.

Horzum, N., Muñoz-Espí, R., Glasser, G., Demir, M.M., Landfester, K., Crespy, D., 2012. Hierarchically structured metal oxide/silica nanofibers by colloid electrospinning. ACS Appl. Mater. Interfaces 4, 6338–6345. https://doi.org/10.1021/am301969w.

Hu, D., Liu, H., Guo, Y., Yang, M., Ma, W., 2022. Interfacial design of nanocellulose/boron nitride nanosheets composites via calcium ion cross-linking for enhanced thermal conductivity and mechanical robustness. Compos Part A Appl Sci Manuf 158. https://doi.org/10.1016/j.compositesa.2022.106970.

Hu, Z., Wang, S., Liu, Y., Qu, Z., Tan, Z., Wu, K., Shi, J., Liang, L., Lu, M., 2020. Constructing a layer-by-layer architecture to prepare a transparent, strong, and thermally conductive boron nitride nanosheet/cellulose nanofiber multilayer film. Ind. Eng. Chem. Res. 59, 4437–4446. https://doi.org/10.1021/acs.iecr.9b05602.

Huang, L., Yu, L., Yin, X., Lin, Y., Xu, Y., Niu, Y., 2022. Silver nanoparticles with vanadium oxide nanowires loaded into electrospun dressings for efficient healing of bacterium-infected wounds. J. Colloid Interface Sci. 622, 117–125. https://doi.org/10.1016/j.jcis.2022.04.026.

Huang, W., Mei, D., Qin, H., Li, J., Wang, L., Ma, X., Zhu, S., Guan, S., 2022. Electrophoretic deposited boron nitride nanosheets-containing chitosan-based coating on Mg alloy for better corrosion resistance, biocompatibility and antibacterial properties. Colloids Surf. A Physicochem. Eng. Asp. 638 https://doi.org/10.1016/j.colsurfa.2022.128303.

Huang, Z.M., Zhang, Y.Z., Kotaki, M., Ramakrishna, S., 2003. A review on polymer nanofibers by electrospinning and their applications in nanocomposites. Compos. Sci. Technol. 63, 2223–2253. https://doi.org/10.1016/S0266-3538(03)00178-7.

Ikram, M., Jahan, I., Haider, A., Hassan, J., Ul-Hamid, A., Imran, M., Haider, J., Shahzadi, A., Shahbaz, A., Ali, S., 2020. Bactericidal behavior of chemically exfoliated boron nitride nanosheets doped with zirconium. Appl. Nanosci. 10, 2339–2349. https://doi.org/10.1007/s13204-020-01412-z.

Jing, L., Li, H., Tay, R.Y., Sun, B., Tsang, S.H., Cometto, O., Lin, J., Teo, E.H.T., Tok, A.I. Y., 2017. Biocompatible hydroxylated boron nitride nanosheets/poly(vinyl alcohol) interpenetrating hydrogels with enhanced mechanical and thermal responses. ACS Nano 11, 3742–3751. https://doi.org/10.1021/acsnano.6b08408.

Kalay, S., Yilmaz, Z., Sen, O., Emanet, M., Kazanc, E., Çulha, M., 2015. Synthesis of boron nitride nanotubes and their applications. Beilstein J. Nanotechnol. https://doi.org/10.3762/bjnano.6.9.

Karakeçili, A.G., Gümüşderelioğlu, M., 2002. Comparison of bacterial and tissue cell initial adhesion on hydrophilic/hydrophobic biomaterials. J. Biomater. Sci. Polym. Ed. 13, 185–196. https://doi.org/10.1163/156856202317414366.

Kaya, B., Zorba, N.N., Caner, C., 2022. Development of novel biodegradable film based on chitosan with borax (sodium tetraborate) and boron nitride and their biological activity. Int. J. Food Sci. Technol. https://doi.org/10.1111/ijfs.15743.

Khan, U., May, P., O'Neill, A., Bell, A.P., Boussac, E., Martin, A., Semple, J., Coleman, J. N., 2013. Polymer reinforcement using liquid-exfoliated boron nitride nanosheets. Nanoscale 5, 581–587. https://doi.org/10.1039/c2nr33049k.

Kim, D., Ha, S., Choi, H.K., Yu, J., Kim, Y.A., 2018. Chemical assembling of amine functionalized boron nitride nanotubes onto polymeric nanofiber film for improving their thermal conductivity. RSC Adv. 8, 4426–4433. https://doi.org/10.1039/c7ra11808b.

Kim, J., Kang, T., Kim, H., Shin, H.J., Oh, S.G., 2019. Preparation of PVA/PAA nanofibers containing thiol-modified silica particles by electrospinning as an eco-friendly Cu (II) adsorbent. J. Ind. Eng. Chem. 77, 273–279. https://doi.org/10.1016/j.jiec.2019.04.048.

Kıvanç, M., Barutca, B., Koparal, A.T., Göncü, Y., Bostancı, S.H., Ay, N., 2018. Effects of hexagonal boron nitride nanoparticles on antimicrobial and antibiofilm activities, cell viability. Mater. Sci. Eng. C 91, 115–124. https://doi.org/10.1016/j.msec.2018.05.028.

Konyashin, I., Loeffler, J., Bill, J., Aldinger, F., 1997. A novel approach to deposition of cubic boron nitride coatings. Thin Solid Films 308–309, 101–106.

Kumeta, K., Nagashima, I., Matsui, S., Mizoguchi, K., 2003. Crosslinking Reaction of Poly (vinyl Alcohol) with Poly(acrylic Acid) (PAA) by Heat Treatment: Effect of Neutralization of PAA.

Laftah, W.A., Hashim, S., Ibrahim, A.N., 2011. Polymer hydrogels: a review. Polym. Plast. Technol. Eng. https://doi.org/10.1080/03602559.2011.593082.

Lahiri, D., Rouzaud, F., Richard, T., Keshri, A.K., Bakshi, S.R., Kos, L., Agarwal, A., 2010. Boron nitride nanotube reinforced polylactide-polycaprolactone copolymer composite: mechanical properties and cytocompatibility with osteoblasts and macrophages in vitro. Acta Biomater. 6, 3524–3533. https://doi.org/10.1016/j.actbio.2010.02.044.

Lahiri, D., Singh, V., Benaduce, A.P., Seal, S., Kos, L., Agarwal, A., 2011. Boron nitride nanotube reinforced hydroxyapatite composite: mechanical and tribological performance and in-vitro biocompatibility to osteoblasts. J. Mech. Behav. Biomed. Mater. 4, 44–56. https://doi.org/10.1016/j.jmbbm.2010.09.005.

Li, D., Xia, Y., 2004. Electrospinning of nanofibers: reinventing the wheel? Advanced materials. https://doi.org/10.1002/adma.200400719.

Li, M., Wang, S., Li, R., Wang, Y., Fan, X., Gong, W., Ma, Y., 2022. The mechanical and antibacterial properties of boron nitride/silver nanocomposite enhanced polymethyl methacrylate resin for application in oral denture bases. Biomimetics 7. https://doi.org/10.3390/biomimetics7030138.

Lee, H., Mensire, R., Cohen, R.E., Rubner, M.F., 2012. Strategies for hydrogen bonding based layer-by-layer assembly of poly(vinyl alcohol) with weak polyacids. Macromolecules 45, 347–355. https://doi.org/10.1021/ma202092w.

Li, R., Guan, X., Lin, X., Guan, P., Zhang, X., Rao, Z., Du, L., Zhao, Jiafeng, Rong, J., Zhao, Jianhao, 2020. Poly(2-hydroxyethyl methacrylate)/β-cyclodextrin-hyaluronan contact lens with tear protein adsorption resistance and sustained drug delivery for ophthalmic diseases. Acta Biomater. 110, 105–118. https://doi.org/10.1016/j.actbio.2020.04.002.

Li, R., Lin, J., Fang, Y., Yu, C., Zhang, Junjie, Xue, Y., Liu, Z., Zhang, Jun, Tang, C., Huang, Y., 2018. Porous boron nitride nanofibers/PVA hydrogels with improved mechanical property and thermal stability. Ceram. Int. 44, 22439–22444. https://doi.org/10.1016/j.ceramint.2018.09.011.

Li, Z., Tang, D., Dai, Y., Zou, R., Liu, H., Tao, Q., Liu, Z., 2022. Fabrication of a novel electrospun polyvinyl alcohol/polyacrylic acid nanofiber adsorbent loading with montmorillonite or zeolite for uranium (VI) removal. J. Radioanal. Nucl. Chem. 331, 297–307. https://doi.org/10.1007/s10967-021-08092-1.

Lim, M., Kim, D., Seo, J., 2016. Enhanced oxygen-barrier and water-resistance properties of poly(vinyl alcohol) blended with poly(acrylic acid) for packaging applications. Polym. Int. 65, 400–406. https://doi.org/10.1002/pi.5068.

Liu, Z., Li, J., Liu, X., 2020. Novel functionalized BN nanosheets/epoxy composites with advanced thermal conductivity and mechanical properties. ACS Appl. Mater. Interfaces 12, 6503–6515. https://doi.org/10.1021/acsami.9b21467.

Merlo, A., Mokkapati, V.R.S.S., Pandit, S., Mijakovic, I., 2018. Boron nitride nanomaterials: biocompatibility and bio-applications. Biomater. Sci. https://doi.org/10.1039/c8bm00516h.

Mukheem, A., Shahabuddin, S., Akbar, N., Miskon, A., Sarih, N.M., Sudesh, K., Khan, N. A., Saidur, R., Sridewi, N., 2019. Boron nitride doped polyhydroxyalkanoate/chitosan nanocomposite for antibacterial and biological applications. Nanomaterials 9. https://doi.org/10.3390/nano9040645.

Naqvi, S.R., Tariq, R., Hameed, Z., Ali, I., Naqvi, M., Chen, W.H., Ceylan, S., Rashid, H., Ahmad, J., Taqvi, S.A., Shahbaz, M., 2019. Pyrolysis of high ash sewage sludge: kinetics and thermodynamic analysis using Coats-Redfern method. Renew. Energy 131, 854–860. https://doi.org/10.1016/j.renene.2018.07.094.

Nisbet, D.R., Forsythe, J.S., Shen, W., Finkelstein, D.I., Horne, M.K., 2009. Review paper: a review of the cellular response on electrospun nanofibers for tissue engineering. J. Biomater. Appl. https://doi.org/10.1177/0885328208099086.

Pan, N., Qin, J., Feng, P., Li, Z., Song, B., 2019. Color-changing smart fibrous materials for naked eye real-time monitoring of wound pH. J. Mater. Chem. B 7, 2626–2633. https://doi.org/10.1039/c9tb00195f.

Pandit, S., Gaska, K., Mokkapati, V.R.S.S., Forsberg, S., Svensson, M., Kádár, R., Mijakovic, I., 2019. Antibacterial effect of boron nitride flakes with controlled orientation in polymer composites. RSC Adv. 9, 33454–33459. https://doi.org/10.1039/c9ra06773f.

Park, J.A., Kang, J.K., Lee, S.C., Kim, S.B., 2017. Electrospun poly(acrylic acid)/poly(vinyl alcohol) nanofibrous adsorbents for Cu(ii) removal from industrial plating wastewater. RSC Adv. 7, 18075–18084. https://doi.org/10.1039/c7ra01362k.

Qu, X.H., Wu, Q., Chen, G.Q., 2006. In vitro study on hemocompatibility and cytocompatibility of poly(3-hydroxybutyrate-co -3-hydroxyhexanoate). J. Biomater. Sci. Polym. Ed. 17, 1107–1121. https://doi.org/10.1163/156856206778530704.

Raza, M., Abu-Jdayil, B., Al-Marzouqi, A.H., Inayat, A., 2022. Kinetic and thermodynamic analyses of date palm surface fibers pyrolysis using Coats-Redfern method. Renew. Energy 183, 67–77. https://doi.org/10.1016/j.renene.2021.10.065.

Santiago-Morales, J., Amariei, G., Letón, P., Rosal, R., 2016. Antimicrobial activity of poly(vinyl alcohol)-poly(acrylic acid) electrospun nanofibers. Colloids Surf. B Biointerfaces 146, 144–151. https://doi.org/10.1016/j.colsurfb.2016.04.052.

Schiffman, J.D., Schauer, C.L., 2008. A review: electrospinning of biopolymer nanofibers and their applications. Polym. Rev. https://doi.org/10.1080/15583720802022182.

Sekkarapatti Ramasamy, M., Rahaman, A., Kim, B., 2021. Influence of oleylamine–functionalized boron nitride nanosheets on the crystalline phases, mechanical and piezoelectric properties of electrospun PVDF nanofibers. Compos. Sci. Technol. 203 https://doi.org/10.1016/j.compscitech.2020.108570.

Serinçay, H., Özkan, S., Yilmaz, N., Koçyiğit, S., Uslu, I., Gürcan, S., Arisoy, M., 2013. PVA/PAA-Based antibacterial wound dressing material with aloe vera. Polym. Plast. Technol. Eng. 52, 1308–1315. https://doi.org/10.1080/03602559.2013.814671.

Shapoval, S.Y., Petrashov, V.T., Popov, O.A., Westner, A.O., Yoder, M.D., Lok, C.K.C., 1990. Cubic boron nitride films deposited by electron cyclotron resonance plasma. Appl. Phys. Lett. 57, 1885–1886. https://doi.org/10.1063/1.104000.

Sridhar, R., Sundarrajan, S., Vanangamudi, A., Singh, G., Matsuura, T., Ramakrishna, S., 2014. Green processing mediated novel polyelectrolyte nanofibers and their antimicrobial evaluation. Macromol. Mater. Eng. 299, 283–289. https://doi.org/10.1002/mame.201300141.

Sun, G., Bi, J., 2021. Scalable production of boron nitride nanosheets in ionic liquids by shear-assisted thermal treatment. Ceram. Int. 47, 7776–7782. https://doi.org/10.1016/j.ceramint.2020.11.122.

Sun, P., Wang, C., He, W., Hou, P., Xu, X., 2017. One-step synthesis of 3D network-like $Ni_xCo_{1-x}MoO_4$ porous nanosheets for high performance battery-type hybrid supercapacitors. ACS Sustain. Chem. Eng. 5, 10139–10147. https://doi.org/10.1021/acssuschemeng.7b02143.

Sundaran, S.P., Reshmi, C.R., Sagitha, P., Manaf, O., Sujith, A., 2019. Multifunctional graphene oxide loaded nanofibrous membrane for removal of dyes and coliform from water. J. Environ. Manag. 240, 494–503. https://doi.org/10.1016/j.jenvman.2019.03.105.

Teo, W.E., Inai, R., Ramakrishna, S., 2011. Technological advances in electrospinning of nanofibers. Sci. Technol. Adv. Mater. https://doi.org/10.1088/1468-6996/12/1/013002.

Tevlek, A., Hosseinian, P., Ogutcu, C., Turk, M., Aydin, H.M., 2017. Bi-layered constructs of poly(glycerol-sebacate)-β-tricalcium phosphate for bone-soft tissue interface applications. Mater. Sci. Eng. C 72, 316–324. https://doi.org/10.1016/j.msec.2016.11.082.

Thomas, M., Enciso, M., Hilder, T.A., 2015. Insertion mechanism and stability of boron nitride nanotubes in lipid bilayers. J. Phys. Chem. B 119, 4929–4936. https://doi.org/10.1021/acs.jpcb.5b00102.

Tian, X., Wu, N., Zhang, B., Wang, Y., Geng, Z., Li, Y., 2021. Glycine functionalized boron nitride nanosheets with improved dispersibility and enhanced interaction with matrix for thermal composites. Chem. Eng. J. 408 https://doi.org/10.1016/j.cej.2020.127360.

Wang, C., Guo, K., He, W., Deng, X., Hou, P., Zhuge, F., Xu, X., Zhai, T., 2017. Hierarchical $CuCo_2O_4$@nickel-cobalt hydroxides core/shell nanoarchitectures for high-performance hybrid supercapacitors. Sci. Bull. 62, 1122–1131. https://doi.org/10.1016/j.scib.2017.08.014.

Wang, J., Planz, V., Vukosavljevic, B., Windbergs, M., 2018. Multifunctional electrospun nanofibers for wound application – novel insights into the control of drug release and antimicrobial activity. Eur. J. Pharm. Biopharm. 129, 175–183. https://doi.org/10.1016/j.ejpb.2018.05.035.

Wang, W., Lin, J., Xing, C., Chai, R., Abbas, S., Song, T., Tang, C., Huang, Y., 2017. Fe_3O_4 nanoparticle-coated boron nitride nanospheres: synthesis, magnetic property and biocompatibility study. Ceram. Int. 43, 6371–6376. https://doi.org/10.1016/j.ceramint.2017.02.047.

Wang, Z., Liu, J., Cheng, Y., Chen, S., Yang, M., Huang, J., Wang, H., Wu, G., Wu, H., 2018. Alignment of boron nitride nanofibers in epoxy composite films for thermal conductivity and dielectric breakdown strength improvement. Nanomaterials 8. https://doi.org/10.3390/nano8040242.

Weng, Q., Wang, Xuebin, Wang, Xi, Bando, Y., Golberg, D., 2016. Functionalized hexagonal boron nitride nanomaterials: emerging properties and applications. Chem. Soc. Rev. https://doi.org/10.1039/c5cs00869g.

Wu, G.M., Lin, S.J., Yang, C.C., 2006. Preparation and characterization of PVA/PAA membranes for solid polymer electrolytes. J. Membr. Sci. 275, 127–133. https://doi.org/10.1016/j.memsci.2005.09.012.

Xi, T., Chen, Y.M., Zheng, Y., Guo, T., Hou, J., Wan, Y., Gao, C., 2009. In vitro cytotoxicity of bacterial cellulose scaffolds used for tissue-engineered bone. J. Bioact. Compat Polym. 24, 137–145. https://doi.org/10.1177/0883911509102710.

Xie, B., Li, C., Chen, J., Wang, N., 2020. Exfoliated 2D hexagonal boron nitride nanosheet stabilized stearic acid as composite phase change materials for thermal energy storage. Sol. Energy 204, 624–634. https://doi.org/10.1016/j.solener.2020.05.004.

Xie, J., Dai, Y., Wang, Youqun, Liu, Yuhui, Zhang, Z., Wang, Yingcai, Tao, Q., Liu, Yunhai, 2021a. Facile immobilization of NiFeAl-LDHs into electrospun poly(vinyl alcohol)/poly(acrylic acid) nanofibers for uranium adsorption. J. Radioanal. Nucl. Chem. 329, 1103–1117. https://doi.org/10.1007/s10967-021-07860-3.

Xie, X., Hou, Z., Duan, G., Zhang, S., Zhou, H., Yang, Z., Zhou, R., 2021b. Boron nitride nanosheets elicit significant hemolytic activity via destruction of red blood cell membranes. Colloids Surf. B Biointerfaces 203. https://doi.org/10.1016/j.colsurfb.2021.111765.

Xiong, R., Hua, D., van Hoeck, J., Berdecka, D., Léger, L., de Munter, S., Fraire, J.C., Raes, L., Harizaj, A., Sauvage, F., Goetgeluk, G., Pille, M., Aalders, J., Belza, J., van Acker, T., Bolea-Fernandez, E., Si, T., Vanhaecke, F., de Vos, W.H., Vandekerckhove, B., van Hengel, J., Raemdonck, K., Huang, C., de Smedt, S.C., Braeckmans, K., 2021. Photothermal nanofibres enable safe engineering of therapeutic cells. Nat. Nanotechnol. 16, 1281–1291. https://doi.org/10.1038/s41565-021-00976-3.

Yadav, H.K.S., Almokdad, A.A., Shaluf, S.I.M., Debe, M.S., 2018. Polymer-based nanomaterials for drug-delivery carriers. In: Nanocarriers for Drug Delivery: Nanoscience and Nanotechnology in Drug Delivery. Elsevier Science Ltd., pp. 531–556. https://doi.org/10.1016/B978-0-12-814033-8.00017-5

Ye, H., Zhang, X., Xu, C., Xu, L., 2019. Few-layer boron nitride nanosheets exfoliated with assistance of fluoro hyperbranched copolymer for poly(vinylidene fluoride-trifluoroethylene) nanocomposite film capacitor. Colloids Surf. A Physicochem. Eng. Asp. 580 https://doi.org/10.1016/j.colsurfa.2019.123735.

Yegin, B., Ozkazanc, H., Er, D.K., Ozkazanc, E., 2022. Antimicrobial performance and charge transport mechanism of Poly(N-methylpyrrole)-boron nitride composite. Mater. Chem. Phys. 278 https://doi.org/10.1016/j.matchemphys.2022.125709.

Yin, C.G., Ma, Y., Liu, Z.J., Fan, J.C., Shi, P.H., Xu, Q.J., Min, Y.L., 2019. Multifunctional boron nitride nanosheet/polymer composite nanofiber membranes. Polymer 162, 100–107. https://doi.org/10.1016/j.polymer.2018.12.038.

Yun, J., Im, J.S., Lee, Y.S., Kim, H. il, 2011. Electro-responsive transdermal drug delivery behavior of PVA/PAA/MWCNT nanofibers. Eur. Polym. J. 47, 1893–1902. https://doi.org/10.1016/j.eurpolymj.2011.07.024.

Zeng, J., Hou, H., Wendorff, J.H., Greiner, A., 2004. Electrospun Poly(vinyl Alcohol)/poly(acrylic Acid) Fibres with Excellent Water-Stability.

Zhan, F., Yan, X., Li, J., Sheng, F., Li, B., 2021. Encapsulation of tangeretin in PVA/PAA crosslinking electrospun fibers by emulsion-electrospinning: morphology characterization, slow-release, and antioxidant activity assessment. Food Chem. 337 https://doi.org/10.1016/j.foodchem.2020.127763.

Zhang, D.L., Zha, J.W., Li, W.K., Li, C.Q., Wang, S.J., Wen, Y., Dang, Z.M., 2018. Enhanced thermal conductivity and mechanical property through boron nitride hot string in polyvinylidene fluoride fibers by electrospinning. Compos. Sci. Technol. 156, 1–7. https://doi.org/10.1016/j.compscitech.2017.12.008.

Zhang, S., Shi, Q., Christodoulatos, C., Meng, X., 2019. Lead and cadmium adsorption by electrospun PVA/PAA nanofibers: batch, spectroscopic, and modeling study. Chemosphere 233, 405–413. https://doi.org/10.1016/j.chemosphere.2019.05.190.

Zhao, H., Ding, J., Xu, B., Zhao, X., Zheng, Y., Shao, Z., Yu, H., 2019. Green synthesis of graphene/boron nitride composites for ultrahigh thermally conductive fluids. ACS Sustain. Chem. Eng. 7, 14266–14272. https://doi.org/10.1021/acssuschemeng.9b03604.

Zhi, C., Bando, Y., Tang, C., Kuwahara, H., Golberg, D., 2009. Large-scale fabrication of boron nitride nanosheets and their utilization in polymeric composites with

improved thermal and mechanical properties. Adv. Mater. 21, 2889–2893. https://doi.org/10.1002/adma.200900323.

Zhou, A., Zhang, Y., Zhang, X., Deng, Y., Huang, D., Huang, C., Qu, Q., 2022. Quaternized chitin/tannic acid bilayers layer-by-layer deposited poly(lactic acid)/polyurethane nanofibrous mats decorated with photoresponsive complex and silver nanoparticles for antibacterial activity. Int. J. Biol. Macromol. 201, 448–457. https://doi.org/10.1016/j.ijbiomac.2022.01.065.

Zhu, M., Hua, D., Pan, H., Wang, F., Manshian, B., Soenen, S.J., Xiong, R., Huang, C., 2018. Green electrospun and crosslinked poly(vinyl alcohol)/poly(acrylic acid) composite membranes for antibacterial effective air filtration. J. Colloid Interface Sci. 511, 411–423. https://doi.org/10.1016/j.jcis.2017.09.101.